



HAL
open science

Distribution of rare earth elements in sediments of the North China Plain: A probe of sedimentation process

Haiyan Liu, Huaming Guo, Olivier Pourret, Zhen Wang, Zhanxue Sun,
Weimin Zhang, Maohan Liu

► **To cite this version:**

Haiyan Liu, Huaming Guo, Olivier Pourret, Zhen Wang, Zhanxue Sun, et al.. Distribution of rare earth elements in sediments of the North China Plain: A probe of sedimentation process. *Applied Geochemistry*, 2021, 134, pp.105089. 10.1016/j.apgeochem.2021.105089 . hal-03332529

HAL Id: hal-03332529

<https://hal.science/hal-03332529>

Submitted on 2 Sep 2021

HAL is a multi-disciplinary open access archive for the deposit and dissemination of scientific research documents, whether they are published or not. The documents may come from teaching and research institutions in France or abroad, or from public or private research centers.

L'archive ouverte pluridisciplinaire **HAL**, est destinée au dépôt et à la diffusion de documents scientifiques de niveau recherche, publiés ou non, émanant des établissements d'enseignement et de recherche français ou étrangers, des laboratoires publics ou privés.

1 **Distribution of rare earth elements in sediments of the North China**

2 **Plain: A probe of sedimentation process**

3
4 Haiyan Liu^{1,2}, Huaming Guo^{3,*}, Olivier Pourret⁴, Zhen Wang^{1,2}, Zhanxue Sun^{1,2},

5 Weimin Zhang^{1,2}, Maohan Liu¹

6
7 ¹ *School of Water Resources and Environmental Engineering, East China University*
8 *of Technology, Nanchang 330013, P. R. China*

9 ² *State Key Laboratory of Nuclear Resources and Environment, East China University*
10 *of Technology, Nanchang 330013, P. R. China*

11 ³ *School of Water Resources and Environment, China University of Geosciences*
12 *(Beijing), Beijing 100083, P.R. China*

13 ⁴ *UniLaSalle, AGHYLE, Beauvais, France*

14
15 *** Corresponding author:** Huaming Guo

16 School of Water Resources and Environment,

17 China University of Geosciences (Beijing),

18 Beijing 100083, P. R. China

19 Tel.: +86-10-8232-1366

20 Fax: +86-10-8232-1081

21 *E-mail address:* hmguo@cugb.edu.cn (H. Guo)

22

23 **Abstract:** Rare earth elements (REE) are powerful tracers for our understanding of
24 sedimentary provenance and depositional processes. This study investigated
25 geochemical characteristics of REE in 226 sediment samples collected from piedmont,
26 central and littoral plains of the North China Plain. Results showed that total REE
27 concentrations exhibited a decreasing trend as piedmont > central > littoral, and 82%,
28 70% and 67% samples had total REE concentrations higher than the value of Upper
29 Continental Crust. The REE concentrations were controlled by sedimentary
30 provenance and sediment physicochemical properties. Ternary diagrams of sandstone
31 classification and Al_2O_3 -CaO+Na₂O-K₂O reflected that sediments originated from
32 greywackes and they experienced an incipient to intermediate chemical weathering.
33 Average Chemical Index of Alteration values were 68, 51 and 55 for sediments from
34 piedmont, central and littoral sediments, respectively. Sediment North American
35 Shale Composite (NASC)-normalized patterns were characterized by light REE
36 (LREE) enrichment over heavy REE (HREE) and coherent negative Eu anomalies
37 (Eu/Eu* ranging between 0.57 and 1.00). Value of (La/Yb)_{NASC} ranged from 0.86 to
38 1.15 (average 1.23), and from 1.03 to 1.49, and from 0.91 to 1.49 in three zones,
39 indicating REE fractionation from piedmont to littoral occurred during sedimentation
40 processes. A positive correlation between (La/Yb)_{NASC} and total REE concentrations
41 was observed in piedmont and central sediment samples, implying that LREE were
42 preferentially enriched over HREE with an accumulation of REE. This positive
43 correlation was not found in littoral sediment samples, where a general decreasing
44 trend along depth for REE concentrations existed. Results of this study shows

45 implications for using REE as a tracer in provenance studies from a basin scale.

46

47 **Keywords: Lanthanides; Geochemistry; Sedimentation; Fractionation; Critical Zone**

48

49 **1. Introduction**

50 Rare earth elements are the lanthanides with atomic numbers ranging from 57
51 (La, lanthanum) to 71 (Lu, lutetium) (Henderson, 1984) as well as yttrium (Y, atomic
52 number 39) and scandium (Sc, atomic number 21; Tyler, 2004). The geochemical
53 signatures of rare earth elements and yttrium (thereafter denoted REE) in sediments
54 and sedimentary rocks are powerful tracers to delineate the geochemical processes.
55 These include magmatism, chemical weathering, diagenesis, erosion and water-rock
56 interactions (McLennan, 1989). As a result, the concentrations and fractionations of
57 REE in sediments and soils have received considerable attention in the past few
58 decades.

59 Numerous investigations have been devoted to studying geochemical behaviors
60 and mobility of REE in sediments and soils, including lake, river and marine
61 sediments (Pourret and Tuduri, 2017; Xu et al., 2018, Wang et al., 2018; Consani et al.,
62 2020), mining surroundings (Hu et al., 2004; Wang and Liang, 2015), wetlands
63 (Davranche et al., 2011; Cheng et al., 2012), agricultural areas (Silva et al., 2015; Han
64 et al., 2017), alluvial deposits (Pédrot et al., 2015; Xie et al., 2014), unconsolidated
65 clay sediments (Guo et al., 2010; Sá Paye et al., 2016) and sedimentary rocks
66 (McLennan, 2001; Šmuc et al., 2012). It's recognized that REE concentrations and
67 distributions in sediments depend on sedimentary provenance and sediment
68 physicochemical properties. Significant correlations between REE concentrations and
69 contents of clay and metals (i.e. Fe, Mn, Al) were observed by Mihajlovic and
70 Rinklebe (2018); while pH value and cation exchange capacity were shown not

71 important factors in their study. Grain size impacted REE concentrations in sediment
72 as well. This is indicated by the results of Kimoto et al. (2006), showing that
73 decreasing grain size generally increased REE concentrations due to that clay
74 minerals could host REE (Laveuf and Cornu, 2009). The impact of clay, silty and sand
75 fractions on solid REE was recently investigated in different soil profiles (Mihajlovic
76 and Rinklebe, 2018). Presence of Fe/Mn oxides was another factor influencing REE
77 in sediments/soils, and more REE can be accumulated by amorphous Fe/Mn oxides as
78 compared to crystalline ones (Yan et al., 1999; Compton et al., 2003).

79 Constituents of REE in sediments and soils for a large part result from natural
80 processes. A global distribution pattern of REE in the soils/sediments was recently
81 evaluated by Adeel et al. (2019), which was achieved using spatial visualization of
82 REE concentration distributions in soils/sediments derived from all over the world.
83 Results obtained from the study showed that total REE concentrations of agriculture
84 soils/sediments ranged from 83 to 9840 mg/kg and concentrations of light REE
85 (LREE) were higher than heavy REE (HREE). This indicates that, in addition to the
86 natural processes, anthropogenic inputs (i.e. fertilizer) contribute to the REE
87 concentrations in sediments/soils in some individual regions. Indeed, fertilization with
88 REE-bearing fertilizers and infiltration of residuals was suggested to be the main
89 mechanism of agriculture-sourced REE entering into soils and sediments (Hu et al.,
90 2004). However, mechanisms for REE mobilization in different soils/sediments and
91 the potential risks of long-term exposure to REE-abundant environment are not
92 adequately understood.

93 Average REE concentration in China's soil was established to be 177 mg/kg
94 (Liang et al., 2005), being comparable to the value (189 mg/kg) of the earth's crust
95 (Wei et al. 1991). China is one of the countries that early widely applied REE in
96 various sectors (Pang et al., 2002; Hu et al., 2006); such as agriculture, the REE have
97 been used as a prompter for crops since 1990s. This has led to high REE pollution
98 levels (i.e. La >80 mg/kg; Nd >85 mg/kg; Sm >45 mg/kg) (Adeel et al., 2019; and
99 references therein). Indeed, sediment and soil contaminations caused by elevated REE
100 have been reported in various regions across China, including in Poyang Lake (Wang
101 et al., 2018), Baotou City (Li et al., 2010), Tibetan Plateau (Wu et al., 2018), Jiaozuo
102 Bay (Zhang and Gao, 2015), Sanjiang Plain (Cheng et al., 2012) and Liaodong Bay
103 (Lin et al., 2013). The North China Plain (NCP) is one of the largest sedimentary
104 basin in Asia (Xing et al., 2013), and is the provincial politics, economy and culture
105 center of China. The plain is characterized by large population (> 0.35 billion) and
106 highly-developed agricultural industry, which plays an important role in the nation's
107 grain manufacture (Chen and Ni, 1987; Kendy et al., 2004). The densely-populated
108 and industrialized areas were shown to be accompanied by increased discharge of
109 REE (i.e. Gd and Sm) into environments (Kulaksız and Bau, 2013; Hatje et al., 2016),
110 due to a large amount of REE applied in industry, medicine as well as agriculture.
111 Studies concerning REE concentrations in sediments of the NCP have been performed
112 (Wei et al., 2010; Liu et al., 2016; Zhang and Gao, 2015; Liu et al., 2019a, b), but a
113 full of investigation of mobility, distributions and behaviors of REE in sediments is
114 still lacking. This would hinder a systematical evaluation of REE levels as well as the

115 possible anthropogenic impact, which is vital for establishing a baseline of
116 distribution and background of REE concentration in the contaminated sediments and
117 for administrating regulation guidelines (Alfaro et al., 2018; Consani et al., 2020).
118 Therefore, the objectives of this study are to: (i) investigate REE concentration and
119 fractionation characteristics in sediments collected from three zones (The zonation
120 was previously specified by Chen et al. (2005)), (ii) characterize the relationships
121 between REE distribution and sediment properties, (iii) assess the feasibility of using
122 REE as a probe of sedimentation process.

123 **2. Material and methods**

124 2.1 Study area

125 The North China Plain (NCP) is located in the eastern China with longitude of
126 $112^{\circ}30'\sim 119^{\circ}30'E$, and latitude of $34^{\circ}46'\sim 40^{\circ}25'N$. The terrains are mostly plains with
127 two mountainous regions (Yanshan and Tanghang mountains) bounding to the north
128 and south, and an oceanic region (Bohai Bay) to the east (Chen et al., 1999),
129 respectively. The plain has a total area of approximately 31×10^4 km² and population
130 of about 0.35 billion inhabitants. The NCP has a semi-arid humid climate with a
131 temperature range of $-23^{\circ}C\sim 42.7^{\circ}C$ (in history). Average annual rainfall ranges from
132 500 mm to 600 mm, mostly (>74%) dominating in summer. Average annual
133 evaporation is 1.5 to 3 times of annual rainfall.

134 The NCP is one of largest sedimentary basins in Asia (Xing et al., 2013).
135 According to Chen et al. (1999), the NCP's geological strata are comprised of four

136 stratigraphic areas: Yinshan-Nuruerhu, Yanshan, Taihangshan and Hebei, with ages
137 ranging from the oldest Archaeozoic to the newest Holocene. Formations in study
138 area have been declining since the Cenozoic due to neotectonics. Geographically, the
139 plain generally decreases from the north to the east with a slope of 0.3‰~0.6‰, and
140 thus it's divided into three zones: piedmont alluvial-proluvial plain, central
141 alluvial-lacustrine plain and littoral plain.

142 Surface sediments in the NCP mainly are Cenozoic deposits with ages from
143 Paleogene to Holocene. Lower Tertiary stratum is composed of red mudstone which is
144 interbedded by red and gray sandstones. Upper Tertiary strata are characterized by
145 consolidated to semi-consolidated alluvial-diluvial deposits, including siltstone,
146 mudstone, sandstone and pebbly sandstone. Quaternary sediments are divided into
147 four groups from top to bottom: Holocene (Q₄), Upper (Q_{3m}), Middle (Q_{2c}) and
148 Lower (Q_{1n}) Pleistocene (Chen, 1999). The Holocene sediments group has a
149 thickness of 5 m to 40 m, and mainly consists of yellow and gray sandy loam, fine
150 sand, clay and sandy gravel. The Upper Pleistocene is alluvial, diluvial and eolian
151 losses and yellow loam. The Middle Pleistocene stratum is widely distributed in
152 intermountain basin and foothills, and consist of red and brown clay, loam and sandy
153 loam, and red mud pebble layers. The Lower Pleistocene sediments group has a
154 buried depth of 350 m to 500 m with a thickness of 80 m to 100m, and it's mainly
155 loam, sand loam and lenticular sand layers.

156 Piedmont alluvial-proluvial sediments are suggested to derive from Taihang and
157 Yanshan mountains by weathering, transport and sedimentation process. Central

158 alluvial-lacustrine sediments are deposited from materials carried by Yellow River
159 and Zhangweinan River running from SW to NE since middle Pleistocene (Shao et al.,
160 1989). The littoral plain forms with interactions between terrene and ocean, and
161 sedimentary deposits come from terrestrial rivers draining into Bohai Bay.

162 2.2 Sediment sampling

163 Sediment samples were taken from three boreholes (Y09, S30 and H02) drilled
164 in three different zones (Fig. 1) of the NCP in the July of 2013. The core sediments
165 were sampled with an interval generally ranging between 1 m and 2 m. Slurries and
166 muds attached on the surface of the core sediments were scrapped off to avoid
167 possible cross contaminations. The samples were parceled with silver paper and were
168 stored in clean plastic bags which were immediately filled with pure N₂ gas for a
169 further preservation. All the sealed core sediments were placed in a shaded
170 environment with temperature below 4 °C during sampling. Finally, the samples were
171 transported to laboratory and preserved in a freezer before analysis.

172 2.3 Sediment analysis

173 All samples used for major and minor constituents analyses were dried under
174 room temperature in the lab, and were ground to grain size <74 μm with an agate
175 mortar for analysis. The X-ray fluorescence (XRF) (ARL Advant X) technique was
176 used for measurement of various oxides (SiO₂, Fe₂O₃, Al₂O₃, MgO, CaO, Na₂O, K₂O,
177 MnO, P₂O₅ and TiO₂) following the national standard method (GB/T 14506).
178 Sediment samples were prepared with a glass flux sheet method. Specifically, 0.7 g

179 (± 0.001) sample was first placed in a 25 mL porcelain crucible; followed by addition
180 of 5.2 g (± 0.001) anhydrous lithium tetraborate, 0.4 g (± 0.001) lithium fluoride and
181 0.3 g (± 0.01) ammonium nitrate, the mixture was evenly stirred. Then the mixture
182 was transferred to a platinum (95%)-gold (5%) alloyed crucible for fusing 10 to 15
183 mins under temperature 1150 to 1250 °C. Finally, fusant was made into glass beads
184 using a fusion machine. All glass beads were preserved in a clean and dry
185 environment before analysis. Reference materials GSS (shown below) were prepared
186 with the same method for subsequent calibration of XRF. The sample intensity (I_s)
187 was calculated by the difference between peak (I_p) and background (I_b) values, as
188 shown with Eq. (2-1).

$$189 \quad I_s = I_p - I_b \quad (2-1)$$

190 Rare earth elements were quantified by employing ICP-MS (AG 7500) with the
191 digested samples. The samples were digested following the method previously
192 described in Liu et al. (2016). Briefly, 9 mL concentrated HCl (37% v/v), 2 mL HNO₃
193 (65% v/v) and 9 mL HF (40% v/v) were used for digesting 0.5 g dried samples for 24
194 h under 108 °C condition. Then the mixture was dried and dissolved again with
195 purified HNO₃ (2% v/v). The obtained solutions were used for REE analysis. To check
196 the stability of the equipment system and the analytical accuracy, reference soil
197 sample including GSS1, GSS2, GSS3 and GSS5, obtained from the Center of China
198 National Standard Reference Material, were ran simultaneously. The recommended
199 and test values of REE and metal oxides in standard references were shown in
200 supplementary materials (Table S1). Furthermore, the parallel sample was performed

201 every ten samples for further monitoring of the analytical precisions. The results show
202 that elements mostly had accuracies (RSD, $\delta 1$) ranging between 2% and 5%. The
203 standard materials had accuracy generally better than 3%, except for P_2O_5 , which had
204 an accuracy better than 8% in some samples. The analytical precisions of REE in all
205 samples were generally better than 5%.

206 2.4 REE normalization

207 Rare earth element concentrations in all sediment samples were normalized with
208 average REE concentrations of the North American Shale Composite (NASC). The
209 corresponding normalization REE values were taken from Taylor and McLennan
210 (1985). Fractionation between LREE and HREE was quantified using fractionation
211 measures $[(La/Lu)_{NASC}$ and $(Nd/Yb)_{NASC}]$. Anomalies including Ce (Ce/Ce^*) and Eu
212 (Eu/Eu^*) were calculated by extrapolation using normalized values of neighboring
213 REE. The corresponding formulas were shown with Eq. (2-1) to (2-4).

$$(La/Lu)_{NASC} = (La_{sample}/La_{NASC})/(Lu_{sample}/Lu_{NASC}) \quad (2-1)$$

$$(Nd/Yb)_{NASC} = (Nd_{sample}/Nd_{NASC})/(Yb_{sample}/Yb_{NASC}) \quad (2-2)$$

$$Ce/Ce^* = Ce_{NASC}/(La_{NASC} \times Pr_{NASC})^{0.5} \quad (2-3)$$

$$Eu/Eu^* = Eu_{NASC}/(Sm_{NASC} \times Gd_{NASC})^{0.5} \quad (2-4)$$

214 where the superscript * indicates the geogenic background.

215 2.5 Calculation of mass transfer coefficient

216 To evaluate REE mobility, the mass transfer coefficient (τ) was calculated by the
217 Eq. (2-5). The $\tau_{i, REE}$ values are an indicator of depletion or enrichment of REE after

218 normalization against reference element i in standard materials (NASC for this study).
219 Positive $\tau_{i, \text{REE}}$ values mean enrichment of REE (total or individual) in the sediments
220 (s) with respect to NASC; negative values indicate depletion and zero indicate REE
221 are immobile. Elements include Fe, Al, Mn, Ti, and Ca can be used as reference
222 element i . This study chooses Ti as the reference because it has been used previously
223 (Wu et al., 2018).

$$\tau_{i, \text{REE}} = (C_{\text{REE}}/C_i)_{\text{sample}} / (C_{\text{REE}}/C_i)_{\text{NASC}} - 1 \quad (2-5)$$

224 **3. Results and discussion**

225 3.1 Sediment geochemistry and provenance

226 Sediment lithology in three boreholes were mainly clay, silt and silty clay (Fig.
227 2). Fine and course sands were generally interbedded with silt and silty clay at
228 different sampling depths. This was well observed in the central (S30) and littoral
229 (H02) borehole bar graphs (Figs. 2b and c). In piedmont borehole, a gravel layer
230 occurred at depth between 38 m and 61 m (Fig. 2a). Gravel was not found in
231 boreholes S30 and HH02. Overall, fine grains prevailed in central and littoral
232 sediment samples. Colors of the fine grains changed in three zones as well. Pale
233 yellow and pale brownish-yellow clay and silty were mainly distributed in piedmont
234 sediments. For central borehole sediments, the color changed from pale
235 brownish-yellow to brown and tan vertically. For littoral sediments, taupe and tawny
236 silty and silty clay were mainly in upper and middle parts, and pale brownish-yellow
237 and pale brown in lower part (Fig. 2c).

238 The component of sediment samples was dominated by SiO_2 (Table 1). For

239 piedmont sediments (borehole Y09), contents (wt%) of SiO₂ ranged from 55.55 to
240 78.36 with an average value of 66.77. Central (borehole S30) and littoral (borehole
241 HH02) sediments had SiO₂ contents (wt%) lower than those of piedmont, being in the
242 ranges of 35.71 to 71.56 (average 56.62) and 32.04 to 77.03 (average 59.51),
243 respectively. Aluminum oxide (Al₂O₃) had the highest contents among the determined
244 metal oxides, with ranges of 6.37 to 14.14 wt%, 7.42 to 13.82 wt% and 7.32 to 15.95
245 wt% and average values of 10.47 wt%, 10.95 wt% and 12.18 wt% in piedmont,
246 central and littoral sediments, respectively. Iron oxide (Fe₂O₃) was the second
247 abundant metal oxides, with a range from 1.86 wt% to 9.86 wt% and an average of
248 5.46 wt% in piedmont sediments. The average content (wt%) of Fe₂O₃ in central and
249 littoral sediments was 4.45 wt% and 4.06 wt%, respectively, exhibiting slightly lower
250 than that of piedmont sediments. Other metal oxides including Na₂O, K₂O, CaO,
251 MgO, P₂O₅ and TiO₂ showed relatively lower content in most of the measured
252 sediment samples as compared to SiO₂ and Al₂O₃ (Table 1). Average value (wt%) of
253 loss on ignition (LOI) was 3.88, 8.56 and 8.02 in piedmont, central and littoral zones
254 with ranges of 1.13 to 7.36, 3.12 to 19.91 and 2.5 to 17.56, respectively.

255 Changes of sediment lithology were controlled by the sedimentary provenances
256 and processes (Bhuiyan et al., 2011; Blake et al., 2017). This would account for that
257 sediments were deposited alternately with clay, silty clay and fine sand (Fig. 2).
258 Terrigenous clastic deposition and land-ocean interactions led to the formation of
259 littoral sedimentation. Weathering and erosion of the bedrocks around the piedmont
260 plain and subsequent transport and sedimentation contributed to the NCP sediments.

261 Ternary diagram of sandstone classification (Blatt et al., 1980) showed that the
262 majority of sediment samples were located in the greywacke domain, and three
263 central samples in the arkose domain indicating that sediments originally mostly were
264 greywacke (Fig. 3a). The dominant SiO₂ contents and fine-grained components
265 reflected that the sedimentary materials had been undergone intensive denudations
266 and a long-distance transport before sink. Indeed, the ternary diagram of
267 Al₂O₃-CaO+Na₂O-K₂O (A-CN-K) showed that the weathering trend of the sediment
268 samples were mostly along the axis of (CaO+Na₂O) (Fig. 3b). This probably indicated
269 that sediment samples from the NCP were in an early weathering stage where
270 minerals such as plagioclase was incongruently decomposed in association with
271 leaching of Na and Ca generating products of illite, kaolinite and smectite (Nesbitt et
272 al., 1980). The offset to the uppermost of K₂O axis was attributed to the addition of
273 terrigenous detrital in the later sedimentary stage (Cox et al., 1995).

274 To quantify the weathering intensity in different samples, the chemical index of
275 alteration (CIA) values (initially was valid for granitic rocks) were calculated
276 following the method proposed by Nesbitt and Young (1982) [CIA = (Al₂O₃/(Al₂O₃ +
277 K₂O + Na₂O + CaO*))×100; CaO* = [CaO - (10/3×P₂O₅) (Panahi et al., 2000)].
278 Chemical index of alteration can be an index reflecting sample in a weathering trend
279 from fresh status to intensely-altered status. Granites and granodiorites usually have
280 CIA values ranging from 45 to 50, and fresh basalts have values between 30 and 45.
281 Muscovite has a value of 75, and illite, montmorillonites and beidellites give values
282 from 75 to 85 (Nesbitt and Young, 1982). Results showed that CIA value of piedmont

283 sediment samples ranged from 55 to 78 with an average value of 68, and central and
284 littoral samples ranged from 37 to 70 (average 51), and from 43 to 70 (average 55),
285 respectively. This indicates that sediment samples were incipiently (CIA: 50 to 60) to
286 intermediately (CIA: 60 to 80) chemically weathered, according to the classification
287 standards suggested by Fedo et al. (1995). It's also observed that piedmont sediment
288 samples generally had higher CIA values as compared to those of central and littoral
289 sediments, which means a stronger weathering may have occurred in the piedmont
290 sediment samples. These differences probably were associated with the
291 hydrogeological conditions such as REE residence time, outcrop lithology and aquifer
292 replenishment conditions (Condie, 1991; Blake et al., 2017). The results were
293 consistent with piedmont samples being located in the upper part of the A-CN-K
294 diagram, while central and littoral sediment samples below the piedmont samples (Fig.
295 3b). The role of chemical weathering on sedimentary processes was studied
296 previously based on sediment geochemical compositions (LaMaskin et al., 2008;
297 Dostal and Keppie, 2009; Xie et al., 2014). Combined to studies of the residence time
298 of REE (Condie, 1991), it's accepted that REE fingerprinting in sediment could serve
299 as a good proxy for understanding the origins and processes of sedimentation, as
300 shown in this investigation.

301 3.2 REE distribution characteristics

302 3.2.1 REE concentrations

303 Total REE (Σ REE) concentrations were shown in Table 1. Piedmont sediment

304 (borehole Y09) Σ REE ranged from 190 mg/kg to 354 mg/kg with an average value of
305 227 mg/kg. Sediments from central (borehole S30) and littoral (borehole H02) zones
306 had Σ REE concentrations ranging from 89 mg/kg to 291 mg/kg (average 183mg/kg)
307 and from 87.90 mg/kg to 238 mg/kg (average 177 mg/kg), respectively. Generally,
308 sediment Σ REE concentrations showed a decreasing trend (piedmont > central >
309 littoral) along a groundwater flow direction. The average Σ REE concentrations in
310 littoral sediment samples from study area were comparable to the values of Upper
311 Continental Crust (UCC) (169 mg/kg) (McLennan, 2001) and Chinese soil (177
312 mg/kg) (Wei et al., 1991); while average Σ REE concentrations of piedmont and
313 central sediments were higher than the values of UCC and soil in China, showing a
314 spatial disparity. All measured average REE concentrations were within in the levels
315 (166 mg/kg to 222 mg/kg) reported in similar researches performed in the same study
316 area (Lan et al., 2016). Others showed that core sediment Σ REE concentrations were
317 slightly higher than the value of surface sediment (Liu et al., 2019b).

318 Sediment Σ REE concentrations varied along depth. In the piedmont borehole,
319 Σ REE concentrations were relatively constant within 11 m below land surface. A
320 small decrease in Σ REE concentrations was observed at depth from 11 m to 16 m
321 before they increased to >300 mg/kg at 25 m. After a new decrease to about 63 m,
322 Σ REE concentrations fluctuated for the remaining sampling depths (Fig. 2a). Σ REE
323 concentrations in central sediments were highly variable along borehole, although a
324 decreasing trend occurred from land surface to 30 m. Vertical changes of Σ REE
325 concentrations were mainly related to sediment physicochemical properties (Kimoto

326 et al., 2006; Mihajlovic and Rinklebe, 2018). Sediments with different grain sizes,
327 such as clay, silt and silty clay, had different capacities in hosting REE. The major
328 minerals in the aquifer sediments of study area were shown to be quartz, K-feldspar,
329 hornblende and calcite accounting for 5%-14% in the piedmont (Chen and Ni, 1987).
330 Clay minerals (i.e. kaolinite, illite and montmorillonite) were more commonly
331 distributed in the central and littoral plains as compared to the piedmont plain (Chen
332 et al., 2005). In the piedmont, where fine sand prevailed (i.e. from 38 m to 62 m),
333 Σ REE concentrations progressively decreased (Fig. 2a). Low Σ REE concentrations of
334 central sediments were found at depth of approximately 30 m, 65 m to 68 m, 107 m,
335 151 m to 154 m, where fine sands were sandwiched with silt and silty clay (Fig. 2b).
336 Silt sand and fine sand more commonly occurred at deeper depth, leading to a
337 decreasing trend of Σ REE concentrations (Fig. 2c). This demonstrated that presence
338 of clay was one of factors controlling Σ REE concentrations. Lanthanides were
339 thought to be hosted by clay component containing in the sediments (Yang et al.,
340 2002). The disparities of clay content along depth for a large part accounted for REE
341 variations along depth. This was supported by the vertical variations of Si/Al values,
342 which were proxies for grain size classification (i.e. clay, silt, and silty clay) (Fig. S2).
343 Statistical analyses showed that Σ REE concentrations were negatively correlated to
344 SiO_2 and were significantly positively correlated to Fe_2O_3 and Al_2O_3 (except for
345 littoral sediment samples) (Table 2), reflecting that REE mainly adsorbed
346 onto/incorporated into Fe and Al-containing clay minerals. Normalization of REE to
347 Ti showed that $\tau_{i, \text{REE}}$ values mostly changed slightly, and generally were positive for

348 piedmont sediments and negative for central and littoral sediment. This suggested that
349 dilution of weathered residuals (i.e. SiO_2) did not significantly modify REE
350 concentrations in sediment samples. Moreover, trends of $\text{SiO}_2/\text{Al}_2\text{O}_3$ values were
351 generally consistent with those of CIA, suggesting that weathering of silicates like
352 feldspar played a role in this process (Fig. 2). In other words, in addition to clay
353 content, Fe and Al-bearing oxides could be another factor influencing REE
354 concentrations in investigated sediment samples. Therefore, mixture of clay minerals
355 and Fe-Mn oxides accounted for normalized REE values. Metal oxides containing Fe,
356 Mn and Al provide important binding sites for sorption of REE (Ohta and Kawabe,
357 2000; Pourret and Davranche, 2013; Liu et al., 2017; Mihajlovic et al., 2019). These
358 findings are in line with the results documented by Wang et al. (2014), showing that
359 fine fractions with abundant clay minerals and Fe/Al/Mn-containing oxides tended to
360 accumulate REE, while coarse fractions with less clay minerals and more quartz led to
361 less REE contents. However, further information on mineralogical compositions of
362 sediment samples is needed for better constraining the impact of mineralogy on REE
363 concentrations from a quantitative perspective. In all, sediment REE concentrations
364 were essentially regulated by their genetic properties and were revealed by their
365 vertical variations.

366 3.2.2 REE fractionation patterns

367 All sediment samples had relatively flat NASC-normalized REE patterns with a
368 gentle enrichment of LREE over HREE (Fig. 4). The degree of LREE enrichment was
369 quantified by $(\text{La}/\text{Yb})_{\text{NASC}}$ values, which ranged between 0.86 and 1.15 with an

370 average of 1.23 in piedmont sediments. Central and littoral sediment samples had
371 $(La/Yb)_{NASC}$ ranges of 1.03 to 1.14 (average 1.21) and 0.91 to 1.49 (average 1.09),
372 respectively (Table 1). Sediments mostly showed negative Ce anomalies with Ce/Ce^*
373 ranging between 0.69 and 1.17 (average 0.91), and between 0.85 and 0.98 (average
374 0.90), and between 0.80 and 0.98 (average 0.89) in piedmont, central and littoral
375 plains, respectively. Negative Eu anomalies commonly occurred in investigated
376 sediments with Eu/Eu^* ranges of 0.82 to 1.07 (average 0.91), 0.83 to 1.31 (average
377 0.95), and 0.86 to 1.34 (average 0.95) in three zones, respectively. Correlation
378 analysis indicated that ΣREE concentrations generally increased with an increase of
379 $(La/Yb)_{NASC}$ in piedmont and central sediments, while this trend was not observed in
380 littoral sediment samples (Fig. 5a). These results reflected REE were nonuniformly
381 accumulated by sediments during their transport. The correlation between
382 $(La/Yb)_{NASC}$ and CIA values showed that the larger $(La/Yb)_{NASC}$ values occurred in
383 samples containing higher ΣREE concentrations and generally having higher CIA
384 values (Fig. 5b). Thus, LREE enrichments could result from the chemical weathering
385 of silicates in crustal materials, which led to higher levels of LREE in sediments
386 (Oliveira et al., 2003; Lin et al., 2013). Larger CIA values were obtained from
387 piedmont and central zones as compared to the values in littoral zones (shown above).
388 The different domains of littoral sediment samples from their piedmont and central
389 counterparts might be related to impact of ocean and/or human activities. However,
390 more studies are needed to verify this speculation.

391 Sediment samples mostly had negative Eu anomalies (Fig. S2). Average Eu/Eu^*

392 anomalies were quite similar in three different zones. This indicated that sedimentary
393 processes, which evolved weathering of bedrocks around plains and migration and
394 deposition in the flat plains, did not fractionate Eu to a larger extent with respect to
395 its neighboring Sm and Gd. Early investigations demonstrated that Eu compositions
396 and distributions in continental crust were fundamentally controlled by shallow,
397 intracrustal differentiation involving Eu-bearing minerals (i.e. plagioclase)
398 (McLennan, 2001), which was shown to possess 4% to 23% (wt) in piedmont
399 sediments (Liu et al., 2016). However, Eu/Eu* values were negatively correlated to
400 Σ REE concentrations (Fig. 5d), suggesting that evolution of Eu anomalies was related
401 to changes of redox conditions as well during sedimentation. Preferential mobilization
402 of Eu(II) over other trivalent REE leads to a segregation of Eu from lanthanide series
403 under reducing conditions (Lee et al., 2003), and hence higher Σ REE concentrations
404 occur in lower-Eu/Eu* samples, as shown in Figure 5d. This mechanism has been
405 proposed for using Eu anomalies as an indicator for investigating REE origins as well
406 as mobility of redox-sensitive metal(oid) (Guo et al., 2010; Davranche et al., 2011).
407 Another possibility resulting in negative correlation between Eu anomalies and Σ REE
408 concentrations would be related to minerals contained in sediments. Such as
409 plagioclase, which tends to preferentially accumulate Eu(II) over trivalent REE by
410 means of isomorphism with Ca^{2+} , Na^{+} and K^{+} (Banks et al., 1999).

411 Cerium anomalies (Ce/Ce^*) were relatively constant in central and littoral
412 sediments despite variable Σ REE concentrations, while they were distributed scattered
413 as a function of Σ REE concentrations in piedmont sediment samples (Fig. S2). The

414 fluctuation of redox conditions could account for this phenomenon due to fact that Ce
415 is readily to be precipitated as insoluble Ce(IV) via oxidative scavenging, and when
416 conditions evolve into reducing, the precipitated Ce will be released into solution by
417 reductive dissolutions (Bau and Koschinsky, 2009; Steinmann and Stille, 2008).
418 Cerium cycle was believed to be biologically mediated (Moffett, 1990; Tanaka et al.,
419 2010) and involved metal (i.e. Fe, Mn) oxides (Yu et al., 2017). Results of our recent
420 study showed that Ce precipitation from oxic aqueous solution was more likely to
421 occur in the piedmont aquifers where low-Fe/Mn-concentration groundwater
422 prevailed (Liu et al., 2019a), though no pronounced positive Ce anomalies were
423 commonly observed in the piedmont aquifer sediments. Thus, both positive and
424 negative Ce anomalies, and no Ce anomalies can be found in solid phases in nature, as
425 the results shown in present study.

426 3.3 Implication for REE signatures

427 Statistical analyses showed that individual REE concentrations were significantly
428 correlated with correlation coefficient (R^2) all better than 0.8. These results, together
429 with the findings that all investigated sediment samples had coherent normalized
430 patterns, indicated that sediments had similar sources/inputs of REE as well as
431 common geochemistry. The remarkable uniformity of sedimentary REE patterns, with
432 absolute concentration ranging from La to Lu, slight LREE enrichment and common
433 negative Eu anomalies, implied that REE were migrated and transported as an integral
434 whole during chemical weathering and sedimentation processes including erosion,
435 sedimentary sorting and diagenesis. The sediment paralleled NASC-normalized REE

436 patterns suggested that REE information recorded in sediments could serve as an ideal
437 tool for studying crustal evolution and sedimentary provenance. The higher REE
438 abundances in sediment than the values of UCC reflected that an enrichment of REE
439 occurred during the process of sedimentation. Since sedimentary REE uniformity was
440 thought to result from effective mixing of various provenance components from the
441 upper crust (McLennan, 2001) and they were transported primarily in particulates, the
442 sedimentary origins and secondary mobilization would be the plausible cause for
443 higher REE abundance. It should be noted that, in addition to natural processes, REE
444 can be accumulated in sediments and soils by various ways including sewage
445 discharges (Verplanck et al., 2005; Hatje et al., 2016), agricultural activities (Alfaro et
446 al., 2018) and atmospheric depositions (Tyler, 2004), although the investigated
447 sediments were unlikely to suffer from these anthropogenic pollutions due to that
448 most of them were not formed nowadays. Positive REE anomalies will show up in
449 REE normalized patterns when individual elemental concentration is greater than its
450 background value, such as Gd anomalies, which have been reported worldwide
451 (Ebrahimi and Barbieri, 2019; and references therein). In summary, sedimentary REE
452 patterns conveys important information regarding the composition of the continental
453 crust and anthropogenic impact.

454 **4. Conclusions**

455 The 226 sediment samples were collected from three different zones (i.e.
456 piedmont, central and littoral) of the north China plain to investigate the
457 concentrations and fractionations of rare earth element (REE). Sediment geochemistry

458 indicated that sediments mostly were derived from greywacke, as suggested by
459 triangular diagram of sandstone classification. All sediment samples had been
460 undergone incipient to intermediate weathering with average CIA of 68, 51 and 55 in
461 three zones, respectively. Total REE concentrations ranged from 190.24 to 353.87
462 mg/kg (average 228.62 mg/kg), and from 88.85 to 290.80 mg/kg (average 182.88
463 mg/kg), and from 87.90 to 237.61 mg/kg (average 176.69 mg/kg) in piedmont, central
464 and littoral plains, exhibiting a decreasing trend as piedmont > central > littoral.
465 Sediment physicochemical properties such as mineral composites and metal oxide
466 abundance controlled REE concentrations, as observed along depth in three sediment
467 sampling profiles. All sediment samples had coherent NASC-normalized REE
468 patterns that were characterized by light REE (LREE) enrichment over heavy REE
469 (HREE) with $(La/Yb)_{NASC}$ ranging between 0.86 and 1.49. Negative Ce and Eu
470 anomalies generally occurred in the investigated sediments with Ce/Ce* and Eu/Eu*
471 ranges of 0.69 to 1.17 and 0.82 to 1.34, respectively. The present study provides
472 important dataset for future comparative studies in this region.

473 **Acknowledgments**

474 This investigation has been funded by National Natural Science Foundation of
475 China (Nos. 41902243, 41222020 and 41172224), National Natural Science
476 Foundation of Jiangxi Province, China (20202BABL211018), the program of China
477 Geology Survey (No. 12120113103700), and the Fok Ying-Tung Education
478 Foundation, China (Grant No. 131017). East China University of Technology
479 Research Foundation for Advanced Talents (Nos. DHBK2019094 and SHT201901).

480 **References**

- 481 Adeel, M., Lee, J. Y., Zain, M., Rizwan, M., Nawab, A., Ahmad, M. A., Shafiq, M., Yi,
482 H., Jilani, G., Javed, R., Horton, R., Rui, Y. K., C. W. Tsang, D. and Xing, B. S.,
483 (2019) Cryptic footprints of rare earth elements on natural resources and living
484 organisms. *Environ. Int.* 127, 785-800.
- 485 Alfaro, M. R., Araújo do Nascimento, C. W., Miranda Biondi, C., da Silva, Y. J. A. B.,
486 de Aguiar Accioly, A. M., Montero, A., Ugarte, O. M. and Esteveze, J. (2018)
487 Rare-earth-element geochemistry in soils developed in different geological
488 settings of Cuba. *Catena* 162, 317-324.
- 489 Banks, D., Hall, G., Reimanna, C. and Siewers, U. (1999). Distribution of rare earth
490 elements in crystalline bedrock groundwaters: Oslo and Bergen regions, Norway.
491 *Appl. Geochem.* 14, 27-39.
- 492 Bau, M. and Koschinsky, A. (2009) Oxidative scavenging of cerium on hydrous Fe
493 oxide: Evidence from the distribution of rare earth elements and yttrium between
494 Fe oxides and Mn oxides in hydrogenetic ferromanganese crusts. *Geochem. J.* 43,
495 37-47.
- 496 Bhuiyan, M. A. H., Rhaman, M. J. J., Dampare, S. B., Suzuki, S. (2011) Provenance,
497 tectonics, and source weathering of modern fluvial sediments of the
498 Brahmaputra-Jamuna River, Bangladesh: inference from geochemistry. *J.*
499 *Geochem. Explor.* 111, 113-137.
- 500 Blake, J. M., Peters, S. C., Johannesson, K. H. (2017) Application of REE
501 geochemical signatures for Mesozoic sediment provenance to the Gettysburg

502 Basin, Pennsylvania. *Sediment. Geol.* 349, 103-111.

503 Blatt, H., Middleton, G. V. and Murray, R. C. (1980) *Origin of Sedimentary Rocks*
504 (2nd edition). New Jersey: Prentice-Hall, 1-634.

505 Chen, W. H. and Ni, M. Y. (1987) *Quaternary Geology in Hebei*. Geological Publish
506 House, Beijing, China. (In Chinese).

507 Chen, W. H. (1999) *Groundwater in Hebei*. Seismological Press, Beijing, (In
508 Chinese).

509 Chen, Z. Y., Nie, Z. L., Zhang, Z. J., Qi, J. X., Nan, Y. J. (2005) Isotopes and
510 sustainability of ground water resources, North China Plain. *Groundwater*, 43,
511 485-493.

512 Cheng, H., Hao, F., Ouyang, W., Liu, S., Lin, C.Y. and Yang, W. (2012) Vertical
513 distribution of rare earth elements in a wetland soil core from the Sanjiang Plain
514 in China. *J. Rare Earth* 30, 731-738.

515 Compton, J. S., White, R. A. and Smith, M. (2003) Rare earth element behavior in
516 soils and salt pan sediments of a semi-arid granitic terrain in the Western Cape,
517 South Africa. *Chem. Geol.* 201 (3-4), 239-255.

518 Condie, K. C. (1991) Another look at rare earth elements in shales. *Geochim.*
519 *Cosmochim. Acta* 55, 2527-2531.

520 Consani, S., Cutroneo, L., Carbone, C. and Capello, M. (2020) Baseline of
521 distribution and origin of Rare Earth Elements in marine sediment of the coastal
522 area of the Eastern Gulf of Tigullio (Ligurian Sea, North-West Italy). *Mar. Pollut.*
523 *Bull.* 155, 111145.

524 Cox, R., Lowe, D. R. and Cullers, R. L. (1995) The influence of sediment recycling
525 and basement composition on evolution of mudrock chemistry in the
526 southwestern United States. *Geochim. Cosmochim. Acta* 59(14), 2919-29440.

527 Davranche, M., Grybos, M., Gruau, G., Pédrot, M., Dia, A. and Marsac, R. (2011)
528 Rare earth element patterns: a tool for identifying trace metal sources during
529 wetland soil reduction. *Chem. Geol.* 284(1-2), 0-137.

530 Dostal, J. and Keppie, J. D. (2009) Geochemistry of low-grade volcanic rocks in the
531 Acatlan Complex of southern Mexico: Evidence for local provenance in
532 felsic-intermediate igneous rocks. *Sediment. Geol.* 222(3-4), 241-253.

533 Ebrahimi, P. and Barbieri, M. (2019) Gadolinium as an emerging microcontaminant in
534 water resources: threats and opportunities. *Geosciences (Switzerland)* 9(2), 93.

535 Fedo, C. M., Nesbitt, H. W., Young and G. M. (1995) Unraveling the effects of
536 potassium metasomatism in sedimentary rocks and paleosols with implications
537 for paleoweathering conditions and provenance. *Geology* 23, 921-924.

538 GB/T 14506. (2010). Methods for chemical analysis of silicate rocks.

539 Guo, H. M., Zhang, B., Wang, G. C. and Shen, Z. L. (2010) Geochemical controls on
540 arsenic and rare earth elements approximately along a groundwater flow path in
541 the shallow aquifer of the Hetao Basin, Inner Mongolia. *Chem. Geol.* 270,
542 117-125.

543 Han, G. L., Song, Z. L. and Tang, Y. (2017) Geochemistry of rare earth elements in
544 soils under different land uses in a typical karst area, Guizhou Province,
545 Southwest China. *Can. J. Soil Sci.* 97, 606-612.

546 Hatje, V., Bruland, K. W. and Flegal, A. R. (2016) Increases in anthropogenic
547 gadolinium anomalies and rare earth element concentrations in San Francisco
548 Bay over a twenty-year record. *Environ. Sci. Technol.* 50, 4159-4168.

549 Henderson, P. (1984) *Rare earth element geochemistry*, Elsevier, Amsterdam.

550 Hu, Z., Richter, H., Sparovek, G. and Schnug, E. (2004) Physiological and
551 biochemical effects of rare earth elements on plants and their agricultural
552 significance: a review. *J. Plant Nutr.* 27, 183-220.

553 Hu, Z. Y., Haneklaus, S., Sparovek, G. and Schnug, E. (2006) Rare earth elements in
554 soils. *Commun. Soil Sci. Plant* 37(9-10), 1381-1420.

555 Kendy, E., Zhang, Y., Liu, C., Wang, J. and Steenhuis, T. (2004) Groundwater
556 recharge from irrigated cropland in the North China Plain: case study of
557 Luancheng County, Hebei Province, 1949-2000. *Hydrol. Process.* 18(12),
558 2289-2302.

559 Kimoto, A., Nearing, M. A., Zhang, X. C. and Powell, D. M. (2006) Applicability of
560 rare earth element oxides as a sediment tracer for coarse-textured soils. *Catena*
561 65 (3), 214-221.

562 Kulaksız, S. and Bau, M. (2013) Anthropogenic dissolved and
563 colloid/nanoparticle-bound samarium, lanthanum and gadolinium in the Rhine
564 River and the impending destruction of the natural rare earth element distribution
565 in rivers. *Earth Planet Sc. Lett.* 362, 43-50.

566 LaMaskin, T. A., Dorsey, R. J. and Vervoort, J. D. (2008) Tectonic controls on
567 mudrock geochemistry Mesozoic rocks of eastern Oregon and western Idaho.

568 U.S.A.:Implications for Cordilleran tectonics. *J. Sediment. Res.* 78(12), 765-783.

569 Lan, X. H., Li, R. H., Mi, B. B., Zhang, Z. X., Guo, X. W. and Long, H. (2016)

570 Distribution characteristics of rare earth elements in surface sediment and their

571 provenance discrimination in the eastern Bohai and northern Yellow Seas. *Earth*

572 *Sci.* 41(3), 462. (In Chinese with English abstract).

573 Laveuf, C. and Cornu, S. (2009) A review on the potentiality of rare earth elements to

574 trace pedogenetic processes. *Geoderma* 154, 1-12.

575 Lee, S. G., Lee, D. H., Kim, Y., Chae, B. G., Kim, W. Y. and Woo, N. C. (2003) Rare

576 earth elements as indicators of groundwater environment changes in a fractured

577 rock system: evidence from fracture-filling calcite. *Appl. Geochem.* 18, 135-143.

578 Li, J., Hong, M., Yin, X. and Liu, J. (2010) Effects of the accumulation of the rare

579 earth elements on soil macrofauna community. *J. Rare Earth* 28, 957-964.

580 Liang, T., Zhang, S., Wang, L. J., Kung, H. T., Wang, Y. Q., Hu, A. T. and Ding, S. M.,

581 (2005) Environmental biogeochemical behaviors of rare earth elements in

582 soil-plant systems. *Environ. Geochem. Health* 27, 301-311.

583 Lin, C. Y., Liu, S. Q., He, M. C. and Li, R. P. (2013) Distribution of rare earth

584 elements in the estuarine and coastal sediments of the daliao river system, China.

585 *J. Radioanal. Nucl. Ch.* 298(1), 627-634.

586 Liu, H. Y., Guo, H. M., Xing, L. N., Zhan, Y. H., Li, F. L., Shao, J. L., N, H., L, X.

587 and Li, C.Q. (2016) Geochemical behaviors of rare earth elements in

588 groundwater along a flow path in the North China Plain. *J. Asian Earth Sci.* 117,

589 33-51.

590 Liu, H. Y, Pourret, O., Guo, H. M. and Bonhoure, J. (2017) Rare earth elements
591 sorption to iron oxyhydroxide: Model development and application to
592 groundwater. *Appl. Geochem.* 87, 158-166.

593 Liu, H. Y., Guo, H. M., Pourret O., Chen, Y. and Yuan, R. X. (2019a) Role of
594 manganese oxyhydroxides in the transport of rare earth elements along a
595 groundwater flow path. *Int. J. Environ. Res. Public Health* 16, 2263.

596 Liu, J., Song, J. M., Yuan, H. M., Li, X. G, Li, N. and Duan, L. Q. (2019b) Rare earth
597 element and yttrium geochemistry in sinking particles and sediments of the
598 Jiaozhou Bay, North China: Potential proxy assessment for sediment
599 resuspension. *Mar. Pollut. Bull.* 144, 79-91.

600 McLennan, S. M. (1989) Rare earth elements in sedimentary rocks: Influence of
601 provenance and sedimentary processes. *Rev. Mineral. Geochem.* 21, 169-200.

602 McLennan, S. M. (2001) Relationships between the trace element composition of
603 sedimentary rocks and upper continental crust. *Geochemistry, Geophysics,*
604 *Geosystems*, 2(4).

605 Mihajlovic, J. and Rinklebe, J. (2018) Rare earth elements in German soils-A review.
606 *Chemosphere* 205(AUG), 514-523.

607 Mihajlovic, J., Bauriegel, A., Stärk, H. J., Roßkopf, N., Zeitz, J., Milbert, G. and
608 Rinklebe, J. (2019) Rare earth elements in soil profiles of various ecosystems
609 across Germany. *Appl. Geochem.* 102, 197-217.

610 Moffett, J. W. (1990) Microbially mediated cerium oxidation in seawater. *Nature* 345,
611 421-423.

612 Nesbitt, H. W., Markovics, G. and Price, R. C. (1980) Chemical processes affecting
613 alkalis and alkaline earths during continental weathering. *Geochim. Cosmochim.*
614 *Acta* 44 (11), 1659-1666.

615 Nesbitt, H. W. and Young, G. M. (1982) Early Proterozoic climates and plate motions
616 inferred from major chemistry of lutites. *Nature*, 299, 19-40.

617 Ohta, A. and Kawabe, I. (2000) Rare earth element partitioning between Fe
618 oxyhydroxide precipitates and aqueous NaCl solutions doped with NaHCO₃:
619 Determinations of rare earth element complexation constants with carbonate ions.
620 *Geochem. J.* 34, 439-454.

621 Oliveira, S. M. B., Larizzatti, F. E., Fávoro, D. I. T., Moreira, S. R. D., Mazzilli, B. P.
622 and Piovano, E. L. (2003) Rare earth element patterns in lake sediments as
623 studied by neutron activation analysis. *J. Radioanal. Nucl. Ch.* 258, 531-535.

624 Panahi, A., Young, G. M and Rainbird, R. H. (2000) Behavior of major and trace
625 elements (including REE) during Paleoproterozoic pedogenesis and diagenetic
626 alteration of an Archean granite near Ville Marie, Québec, Canada. *Geochim.*
627 *Cosmochim. Acta* 64(13), 2199-2220.

628 Pang, X., Li, D. and Peng, A. (2002) Application of rare-earth elements in the
629 agriculture of China and its environmental behavior in soil. *Environ. Sci. Pollut.*
630 *Res.* 9, 143-148.

631 Pourret, O. and Davranche, M. (2013) Rare earth element sorption onto hydrous
632 manganese oxide: A modeling study. *J. Colloid Interf. Sci.* 395, 18-23.

633 Pourret, O. and Tuduri, J. (2017) Continental shelves as potential resource of rare

634 earth elements. *Sci. Rep.* 7, 585.

635 Pédrot, M., Dia, A., Davranche, M. and Gruau, G. (2015) Upper soil horizons control
636 the rare earth element patterns in shallow groundwater. *Geoderma*, 239-240,
637 84-96.

638 Salmanighabeshi, S., Palomo-Marín, M. R., Bernalte, E., Rueda-Holgado, F.,
639 Miró-Rodríguez, C., Fadic-Ruiz, X., Vidal-Cortez, V., Cereceda-Balic, F.,
640 Pinilla-Gil, E. (2015). Long-term assessment of ecological risk from deposition
641 of elemental pollutants in the vicinity of the industrial area of
642 Puchuncaví-Ventanas, central Chile. *Sci Total Environ* 527-528: 335-43.

643 Sá Paye, H., de Mello, J. W. V., de Magalhães Mascarenhas, G. R. L., de and
644 Gasparon, M. (2016) Distribution and fractionation of the rare earth elements in
645 Brazilian soils. *J. Geochem. Explor.* 161, 27-41.

646 Shao, S. X., Guo, S. Q. and Han, S. H. (1989) Geomorphical structures and evolution
647 of the Huanghuaihai plain in China. *Acta Geosci. Sin.* 44(3), 314-322.

648 Silva, Y. J. A. B., Cantalice, J. R. B., Singh, V. P., Nascimento, C. W. A., Piscoya, V. C.
649 and Guerra, S. M. S. (2015) Trace element fluxes in sediments of an
650 environmentally impacted. *Environ. Sci. Pollut. Res.* 22, 14755-14766.

651 Steinmann, M. and Stille, P. (2008) Controls on transport and fractionation of the rare
652 earth elements in stream water of a mixed basaltic-granitic catchment basin
653 (Massif Central, France). *Chem. Geol.* 254(1), 1-18.

654 Šmuc, N. R., Dolenc, T., Serafimovski, T., Dolenc, M. and Vrhovnik, P. (2012)
655 Geochemical characteristics of rare earth elements (REEs) in the paddy soil and

656 rice (*Oryza sativa* L.) system of Kočani Field, Republic of Macedonia.
657 Geoderma, 183-184, 1-11.

658 Tanaka, K., Tani, Y., Takahashi, Y., Tanimizu, M., Suzuki, Y., Kozai, N. and Ohnuki, T.
659 (2010) A specific Ce oxidation process during sorption of rare earth elements on
660 biogenic Mn oxide produced by *Acremonium* sp. Strain KR21-2. *Geochim.*
661 *Cosmochim. Acta* 74, 5463-5477.

662 Taylor, S. R. and McLennan, S. M. (1985) *The Continental Crust: Its Composition*
663 *and Evolution*. Blackwell, Boston, 312 pp.

664 Tyler, G. (2004) Rare earth elements in soil and plant systems-a review. *Plant and Soil*.
665 267 (1-2), 191-206.

666 Verplanck, P. P., Taylor, H. E., Nordstrom, D. K. and Barber, L. B. (2005) Aqueous
667 Stability of Gadolinium in Surface Waters Receiving Sewage Treatment Plant
668 Effluent, Boulder Creek, Colorado. *Environ. Sci. Technol.* 39 (18), 6923-6929.

669 Wang, S. H., Zhang, N., Chen, H., Li, L., Yan, W. (2014) The surface sediment type
670 and their rare earth element characteristics from the continental shelf of the
671 northern South China Sea. *Cont. Shelf Res.* 88, 185-202.

672 Wang, L. and Liang, T. (2015) Geochemical fractions of rare earth elements in soil
673 around a mine tailing in Baotou, China. *Sci. Rep.* 5, 12483.

674 Wang, L., Han, X., Liang, T., Guo, Q., Li, J., Dai, L. and Ding, S. (2018)
675 Discrimination of rare earth element geochemistry and co-occurrence in
676 sediment from Poyang Lake, the largest freshwater lake in China. *Chemosphere*
677 217, 851-857.

- 678 Wei, L., Guo, H. M., Xie, Z. H. and Li, Z. P. (2010) Rare earth elements geochemistry
679 and its implication for sediment provenance in the Beijing plain, *Earth Sci. Front.*
680 17(6), 72-80. (In Chinese with English abstract).
- 681 Wei, F. S., Liu, T. L., Teng, E. J. and Rui, K. S. (1991) A survey on the background
682 contents of 15 rare earth elements in Chinese soil. *Environ. Sci.* 12, 78-82 (In
683 Chinese with English abstract).
- 684 Wu, J., Lu, J., Li, L. M., Min, X. Y., Zhang, Z. H. and Luo Y. M. (2018) Distribution,
685 pollution, and ecological risks of rare earth elements in soil of the northeastern
686 Qinghai-tibet plateau. *Hum. Ecol. Risk Assess.* 25(3), 1-16.
- 687 Xie, X. J., Wang, Y. X., Ellis, A., Liu, C. X., Duan, M. Y. and Li, J. X. (2014) Impact
688 of sedimentary provenance and weathering on arsenic distribution in aquifers of
689 the Datong basin, China: Constraints from elemental geochemistry. *J. Hydrol.*
690 519, 3541-3549.
- 691 Xing, L. N., Guo, H. M. and Zhan, Y. H. (2013) Groundwater hydrochemical
692 characteristics and processes along flow paths in the North China Plain. *J. Asian*
693 *Earth Sci.* 70-71, 250-264.
- 694 Xu, N., Morgan, B. and W. Rate, A. (2018) From source to sink: Rare-earth elements
695 trace the legacy of sulfuric dredge spoils on estuarine sediments. *Sci. Total*
696 *Environ.* 637-638, 1537-1549.
- 697 Yan, X. P., Kerrich, R. and Hendry, M. J. (1999) Sequential leachates of multiple
698 grain size fractions from a clay-rich till, Saskatchewan, Canada: implications for
699 controls on the rare earth element geochemistry of porewaters in an aquitard.

700 Chem. Geol. 158, 53-79.

701 Yang, S. Y., Jung, H. S., Choi, M. S. and Li, C. X. (2002) The rare earth element
702 compositions of the Changjiang (Yangtze) and Huanghe (Yellow) river sediments.
703 Earth Planet Sc. Lett. 201, 407-419.

704 Yu, C., Drake, H., Mathurin, F. A. and Åström, M. E. (2017) Cerium sequestration
705 and accumulation in fractured crystalline bedrock: The role of Mn-Fe (hydr-)
706 oxides and clay minerals. Geochim. Cosmochim. Acta 199, 370-389.

707 Zhang, Y. and Gao, X. L. (2015) Rare earth elements in surface sediments of a marine
708 coast under heavy anthropogenic influence: The Bohai Bay, China. Estuar.
709 Coastal Shelf S. 164, 86-93.

710

711 **Figure and Table captions**

712 **Table 1** Concentrations of REE and major oxides and REE fractionation indices in the
713 sediment samples from three zones

714 **Table 2** Pearson's correlations between REE concentrations and major oxides, CIA
715 and LOI in the sediment samples from three zones (Y09 (118 m): piedmont, n = 50;
716 S30 (184 m): central, n=163; H02 (110 m): littoral, n = 63; "***" indicates $p < 0.01$,
717 "*" $p < 0.05$)

718 **Figure 1** Study area and sediments sampling locations (boreholes)

719 **Figure 2** Changes of sediment lithology and REE parameters along depth: (a)
720 piedmont borehole Y09, (b) central borehole S30, (c) littoral borehole H02

721 **Figure 3** Ternary diagram of sandstone classification and Al_2O_3 -CaO+Na₂O-K₂O
722 (A-CN-K)

723 **Figure 4** NASC-normalized REE patterns and absolute REE concentrations in all
724 sediment samples (The line indicates a trend of normalized REE concentrations. The
725 box-whisker shows distributions of absolute REE concentrations; (a) piedmont
726 borehole Y09, (b) central borehole S30, (c) littoral borehole H02)

727 **Figure 5** Total REE concentrations as a function of $(La/Yb)_{NASC}$ (a), Ce/Ce^* (c) and
728 Eu/Eu^* (d); a relationship between CIA and $(La/Yb)_{NASC}$ (b)

729

730

731

732

Table 1

Component	Unit	piedmont			central			littoral		
		Y09			S30			H02		
		Min.	Avg.	Max.	Min.	Avg.	Max.	Min.	Avg.	Max.
La	mg/kg	19.54	40.93	63.81	16.59	33.16	54.53	16.80	32.05	43.99
Ce	mg/kg	39.75	82.99	135.94	31.99	66.34	108.59	31.81	63.09	87.26
Pr	mg/kg	4.60	9.71	14.98	3.87	7.72	12.38	3.87	7.39	10.01
Nd	mg/kg	16.50	35.71	55.46	13.96	28.41	45.28	13.70	27.28	36.75
Sm	mg/kg	3.12	6.81	10.43	2.66	5.56	8.73	2.58	5.40	7.30
Eu	mg/kg	0.70	1.31	1.91	0.72	1.12	1.60	0.72	1.09	1.50
Gd	mg/kg	2.73	6.09	9.67	2.32	4.99	7.72	2.22	4.87	6.97
Tb	mg/kg	0.45	0.97	1.52	0.34	0.78	1.24	0.34	0.78	1.10
Dy	mg/kg	2.49	5.41	8.35	1.97	4.34	6.75	1.97	4.32	6.03
Ho	mg/kg	0.55	1.11	1.70	0.40	0.88	1.35	0.41	0.88	1.22
Er	mg/kg	1.53	3.10	4.42	1.11	2.46	3.72	1.08	2.47	3.40
Tm	mg/kg	0.26	0.53	0.75	0.19	0.42	0.64	0.20	0.43	0.59
Yb	mg/kg	1.59	3.20	4.47	1.24	2.64	3.93	1.18	2.62	3.50
Lu	mg/kg	0.27	0.53	0.73	0.20	0.44	0.66	0.21	0.44	0.60
Y	mg/kg	14.60	30.20	44.94	10.53	23.61	36.11	10.80	23.59	34.05
SiO ₂	wt%	55.55	66.77	78.36	35.71	56.62	71.56	32.04	59.51	77.03
Fe ₂ O ₃	wt%	1.86	5.46	9.86	2.00	4.45	6.51	1.83	4.06	6.61
Al ₂ O ₃	wt%	6.37	10.47	14.14	7.42	10.95	13.82	7.32	12.18	15.96
MgO	wt%	0.27	1.38	2.41	1.01	2.34	3.70	0.61	2.14	5.27
CaO	wt%	0.40	1.25	5.45	0.97	7.01	19.23	1.30	6.12	18.63
Na ₂ O	wt%	0.15	1.15	2.28	0.66	1.65	3.31	0.52	3.38	46.29
K ₂ O	wt%	1.89	2.58	3.37	1.55	2.20	2.82	1.57	2.26	2.89
MnO	wt%	0.02	0.07	0.30	0.03	0.07	0.15	0.04	0.07	0.16
P ₂ O ₅	wt%	0.06	0.1	0.69	0.13	0.25	0.36	0.04	0.12	0.17
TiO ₂	wt%	0.26	0.69	0.99	0.44	0.93	1.54	0.51	0.96	1.22
LOI	wt%	1.13	3.88	7.36	3.12	8.56	19.91	2.5	8.02	17.56
∑REE	mg/kg	109	229	354	89	183	291	88	177	238
LREE	mg/kg	84	178	279	70	142	231	7	136	183
HREE	mg/kg	9.93	20.94	31.59	7.77	16.96	26.00	7.61	16.81	23.39
LREE/HREE	-	6.93	8.43	10.83	7.51	8.36	9.69	7.33	8.15	9.80
Ce/Ce*	-	0.69	0.91	1.17	0.85	0.90	0.98	0.80	0.89	0.98
Eu/Eu*	-	0.82	0.91	1.07	0.83	0.95	1.31	0.86	0.95	1.34
Gd/Gd*	-	0.95	1.06	1.15	0.93	1.05	1.12	0.87	1.04	1.10
(Y/Ho) _{NASC}	-	1.09	1.13	1.22	1.04	1.11	1.17	1.06	1.11	1.19
(La/Yb) _{NASC}	-	0.86	1.23	1.15	1.03	1.21	1.49	0.91	1.09	1.49

Table 2

	borehole	REE	SiO ₂	Fe ₂ O ₃	Al ₂ O ₃	MgO	CaO	Na ₂ O	K ₂ O	LOI	CIA
REE	Y09	1									
	S30	1									
	H02	1									
SiO ₂	Y09	-0.79**	1								
	S30	-0.58**	1								
	H02	-0.67**	1								
Fe ₂ O ₃	Y09	0.72**	-0.92**	1							
	S30	0.90**	-0.56**	1							
	H02	0.89**	-0.67**	1							
Al ₂ O ₃	Y09	0.67**	-0.77**	0.85**	1						
	S30	0.51**	0.249**	0.60**	1						
	H02	0.19	0.430**	0.30*	1						
MgO	Y09	0.55**	-0.77**	0.79**	0.55**	1					
	S30	0.66**	-0.61**	0.79**	0.31**	1					
	H02	0.71**	-0.84**	0.71**	-0.32**	1					
CaO	Y09	-0.06	-0.11	0.05	-0.342*	0.44**	1				
	S30	0.12	-0.82**	0.04	-0.72**	0.21*	1				
	H02	0.15	-0.58**	0.06	-0.40**	0.12	1				
Na ₂ O	Y09	-0.74**	0.78**	-0.70**	-0.79**	-0.31*	0.31*	1			
	S30	-0.81**	0.79**	-0.75**	-0.24*	-0.57**	-0.44**	1			

	H02	0.19	-0.51**	0.13	-0.76**	0.68**	-0.07	1			
K ₂ O	Y09	0.13	-0.09	0.001	-0.125	-0.19	-0.40**	-0.18	1		
	S30	0.17	0.26**	0.36**	0.58**	0.17	-0.61**	0.09	1		
	H02	0.17	-0.003	0.46**	0.49**	0.08	-0.39**	-0.19	1		
LOI	Y09	0.50**	-0.84**	0.60**	0.46**	0.44**	0.03	-0.52**	-0.003	1	
	S30	0.21*	0.91**	0.16	0.64**	0.23*	0.83**	0.52**	1.74	1	
	H02	0.27*	0.85**	0.25*	0.47**	0.42**	0.62**	-0.04	-0.03	1	
CIA	Y09	0.51**	-0.75**	0.82**	0.54**	0.44**	-0.003	-0.66**	-0.04**	0.56**	1
	S30	0.26	0.06	0.36**	0.02	0.09	-0.52**	-0.06	0.34**	0.002	1
	H02	0.35**	0.03	0.48**	0.25*	0.26*	-0.29*	-0.01	0.21*	-0.01	1

736

737

738

739

740

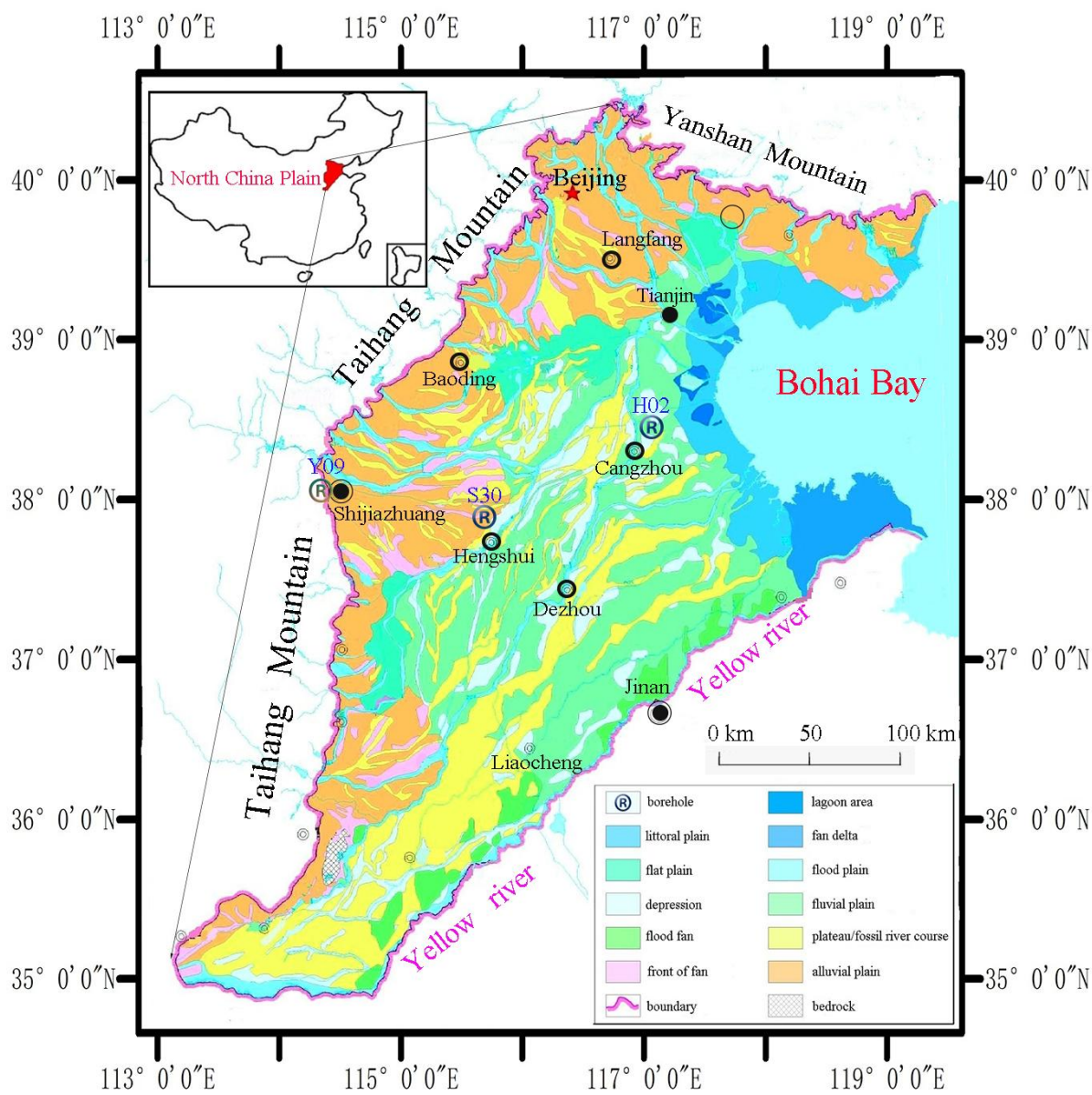


Fig. 1

741
 742
 743
 744
 745
 746
 747

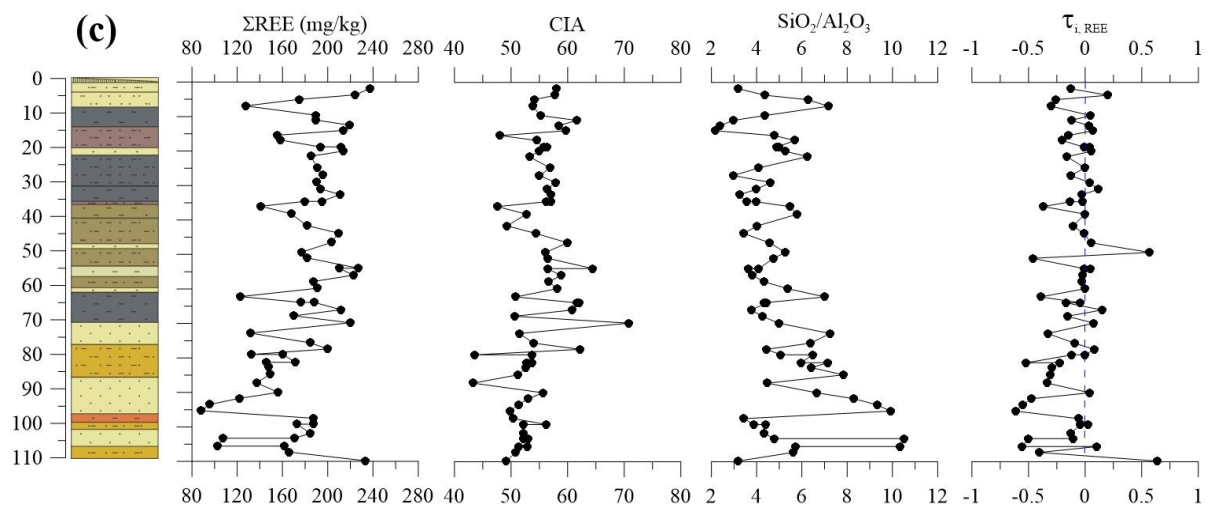
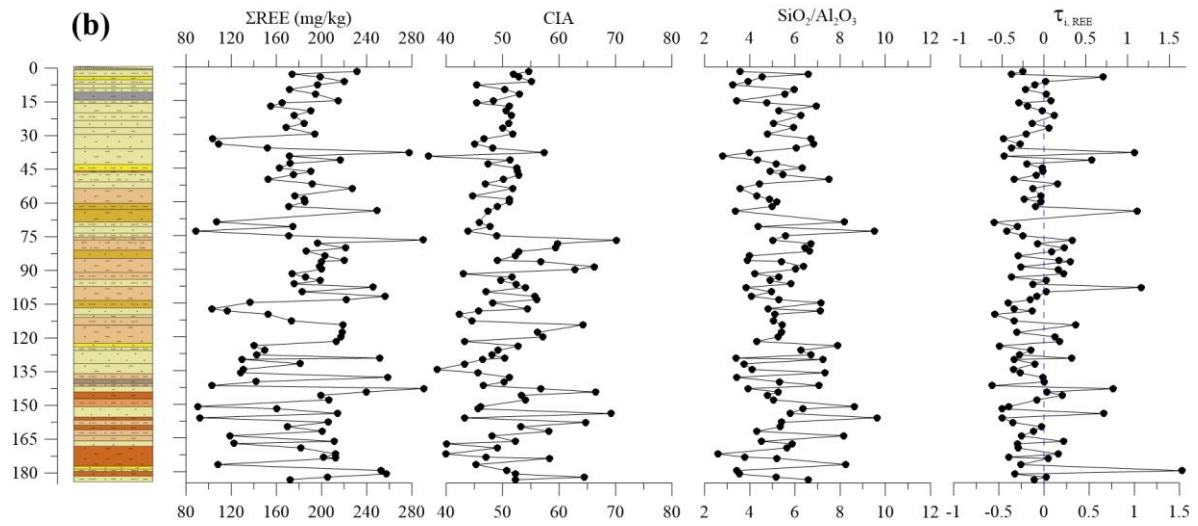
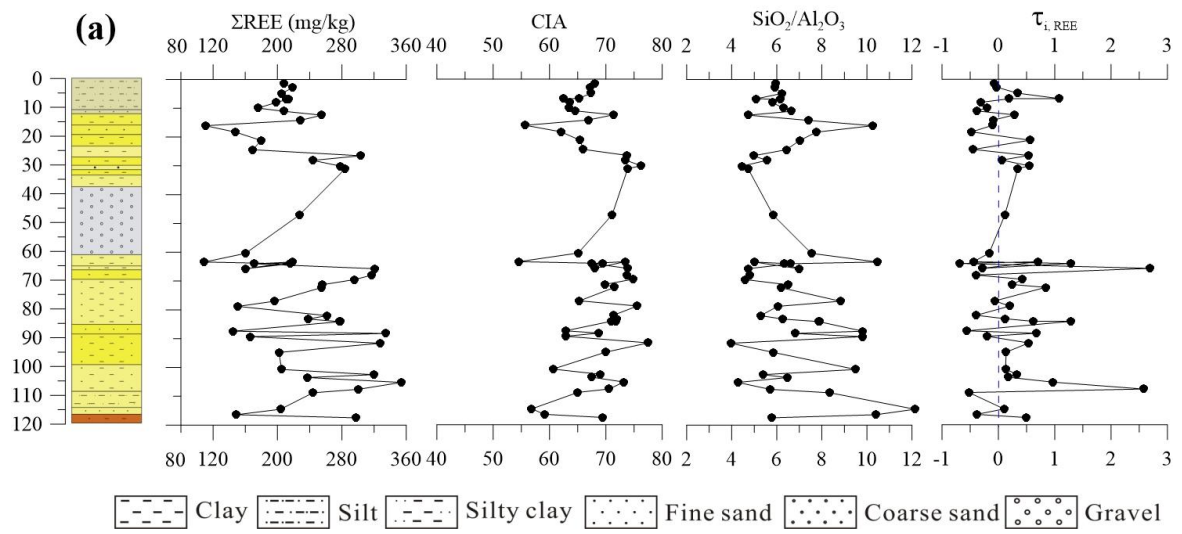


Fig. 2

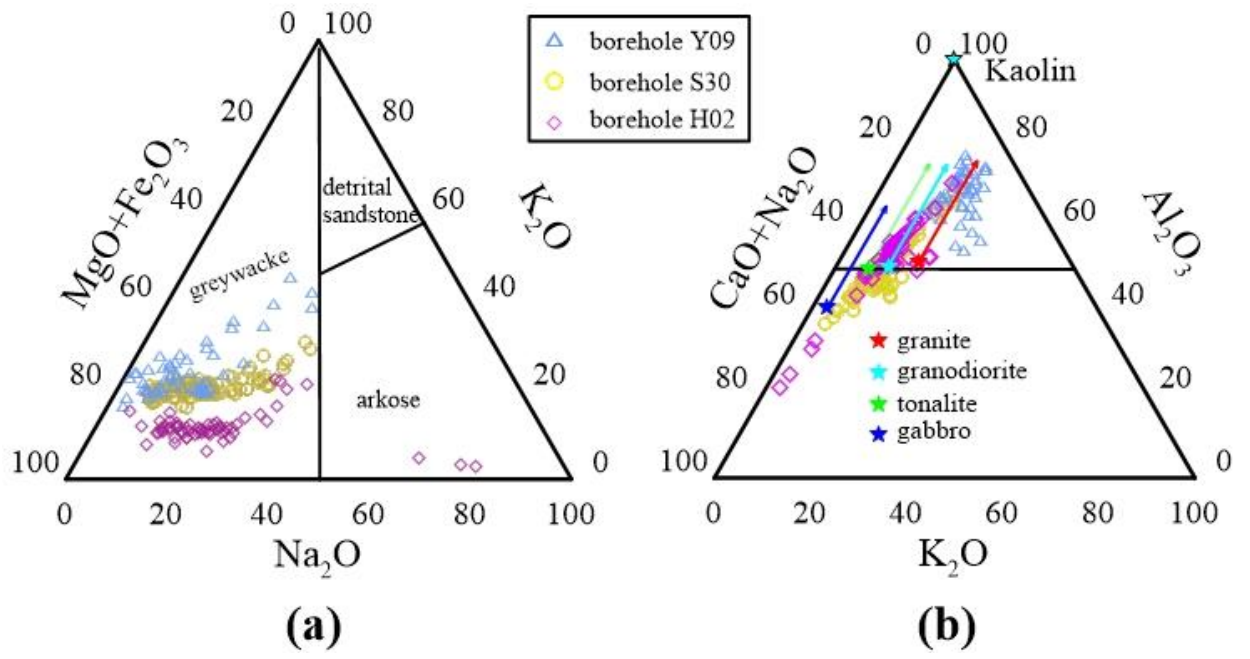


Fig. 3

754
 755
 756
 757
 758
 759
 760

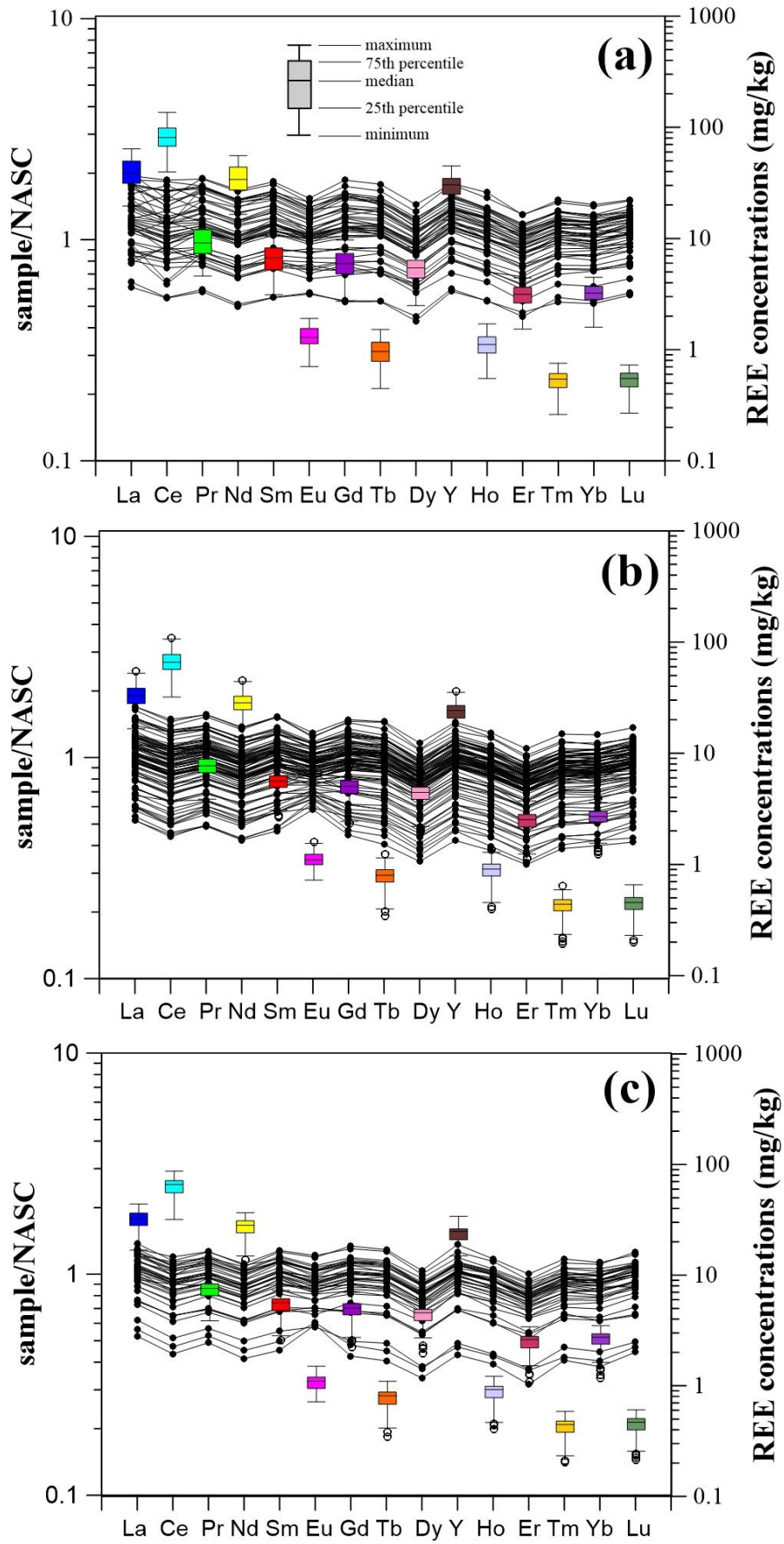
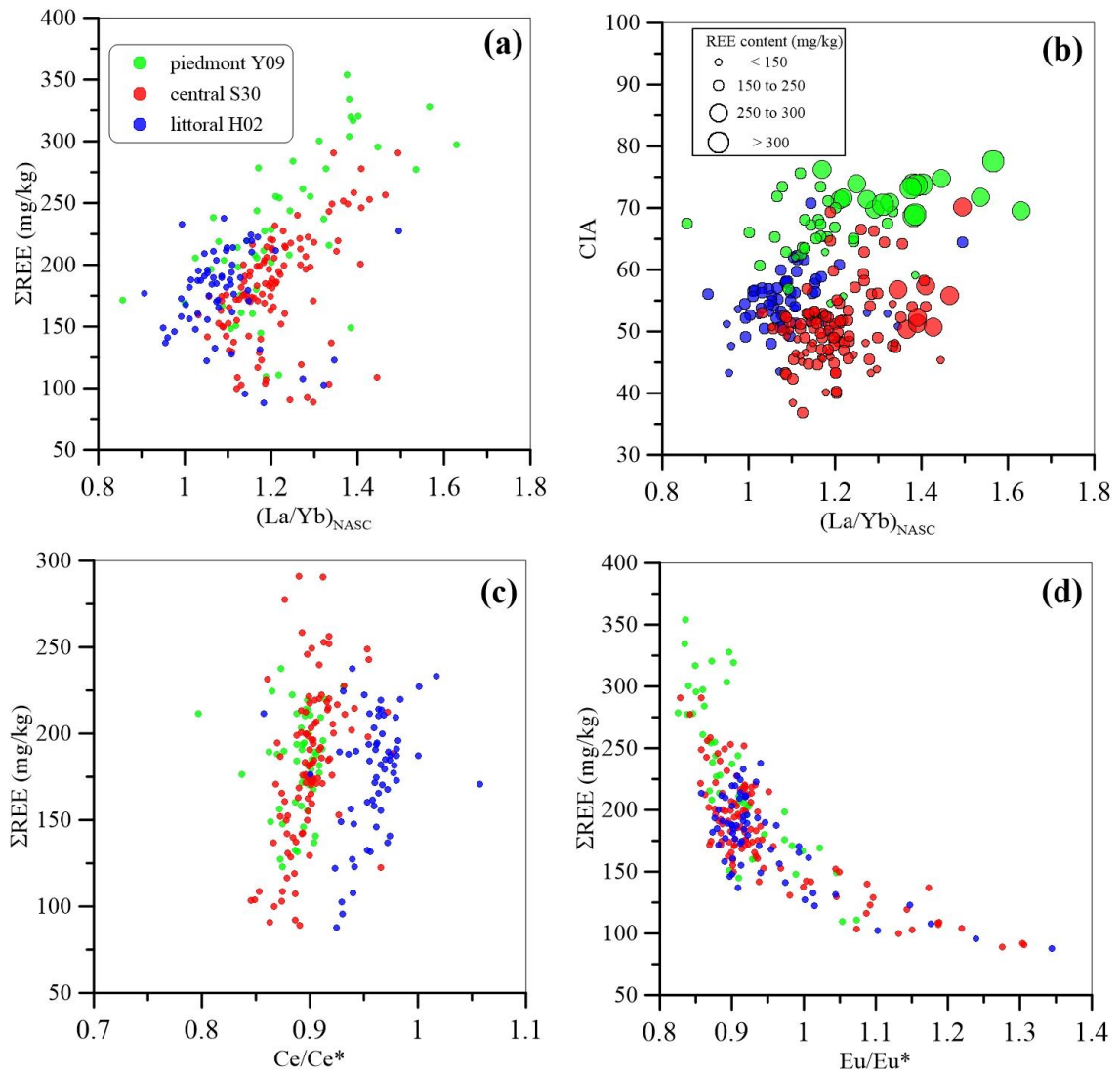


Fig. 4

761

762

763
764



765
766
767
768
769
770
771

Fig. 5